Original Article

Metal artifacts from titanium and steel screws in CT, 1.5T and 3T MR images of the tibial Pilon: a quantitative assessment in 3D

Shairah Radzi[1], Gary Cowin[2], Mark Robinson[3], Jit Pratap[4], Andrew Volp[4], Michael A. Schuetz[1,5], Beat Schmutz[1]

[1]Institute of Health and Biomedical Innovation, Queensland University of Technology, QLD 4059, Australia; [2]Centre of Advanced Imaging, University of Queensland, QLD 4072, Australia; [3]Orthopaedics Department, Royal Brisbane and Women's Hospital, QLD 4006, Australia; [4]Radiology Department, [5]Trauma Services, Princess Alexandra Hospital, QLD 4102, Australia

Correspondence to: Dr. Beat Schmutz. Institute of Health and Biomedical Innovation, Queensland University of Technology, 60 Musk Avenue, Kelvin Grove, QLD 4059, Australia. Email: b.schmutz@qut.edu.au.

Abstract: Radiographs are commonly used to assess articular reduction of the distal tibia (pilon) fractures postoperatively, but may reveal malreductions inaccurately. While magnetic resonance imaging (MRI) and computed tomography (CT) are potential three-dimensional (3D) alternatives they generate metal-related artifacts. This study aims to quantify the artifact size from orthopaedic screws using CT, 1.5T and 3T MRI data. Three screws were inserted into one intact human cadaver ankle specimen proximal to and along the distal articular surface, then CT, 1.5T and 3T MRI scanned. Four types of screws were investigated: titanium alloy (TA), stainless steel (SS) (Ø =3.5 mm), cannulated TA (CTA) and cannulated SS (CSS) (Ø =4.0 mm, Ø empty core =2.6 mm). 3D artifact models were reconstructed using adaptive thresholding. The artifact size was measured by calculating the perpendicular distance from the central screw axis to the boundary of the artifact in four anatomical directions with respect to the distal tibia. The artifact sizes (in the order of TA, SS, CTA and CSS) from CT were 2.0, 2.6, 1.6 and 2.0 mm; from 1.5T MRI they were 3.7, 10.9, 2.9, and 9 mm; and 3T MRI they were 4.4, 15.3, 3.8, and 11.6 mm respectively. Therefore, CT can be used as long as the screws are at a safe distance of about 2 mm from the articular surface. MRI can be used if the screws are at least 3 mm away from the articular surface except for SS and CSS. Artifacts from steel screws were too large thus obstructed the pilon from being visualised in MRI. Significant differences ($P<0.05$) were found in the size of artifacts between all imaging modalities, screw types and material types, except 1.5T versus 3T MRI for the SS screws ($P=0.063$). CTA screws near the joint surface can improve postoperative assessment in CT and MRI. MRI presents a favourable non-ionising alternative when using titanium hardware. Since these factors may influence the quality of postoperative assessment, potential improvements in operative techniques should be considered.

Keywords: Computed tomography (CT); metal artifacts; magnetic resonance imaging (MRI); pilon; tibial plafond

Submitted Jan 28, 2014. Accepted for publication Mar 14, 2014.
doi: 10.3978/j.issn.2223-4292.2014.03.06
View this article at: http://www.amepc.org/qims/article/view/3553/4700

Introduction

Intraarticular fractures of the distal tibia (pilon) are among the most complex injuries of the lower limb (1). Achieving anatomical reduction of the fragments is technically difficult and sometimes impossible, even for the experienced surgeon (2). Plain film radiographs are traditionally used to assess the quality of anatomical reduction of pilon fractures after open reduction and internal fixation. However, they have been shown to poorly demonstrate articular incongruities of the tibial pilon, especially in the rotational and translational alignment of the malreduced fragments (3,4). Other studies have also shown similar findings for tibial plateau (5) and acetabulum fractures (6). In addition, depending on the severity of the fracture, location of

orthopaedic implants used, and the position of the ankle at the time the radiographic examination is conducted, fracture fixation plates and screws may obstruct the features of the articular alignment (7) and can be over-projected (8), thus does not allow clinicians to visually assess the quality of joint reduction accurately. Moreover, plain radiographs are projected in 2D, therefore cannot help distinguish the subchondral lines of reduced and non-reduced individual fragments, since the distal articular surface is three-dimensional (3D) in reality.

Nevertheless, it is important to assess the quality of the articular reduction as studies have shown that irregular load distributions in the articular surface resulting from malreduced fragments can contribute to posttraumatic arthritis (9), sclerosis and osteophyte formation (10). Other medical imaging modalities such as computed tomography (CT) and magnetic resonance imaging (MRI) are alternatives to radiographs as they can produce 3D volumetric datasets of bones and its articular surfaces.

However, due to burden on facilities, increased radiation exposure and costs compared to radiographs, postoperative CT scans of pilon fractures are only obtained for complex cases and not conducted on a routine basis. MRI on the other hand is non-radiation based and provides superior imaging of the cartilage and other soft tissue structures. Although the use of MRI has primarily been on the assessment of soft tissue injuries of the ankle (11), two recent studies by the authors have shown that MRI based 3D models of long bones are of comparable accuracy to those generated from CT data (12,13). Most of the modern commercial fracture fixation implants do not contain any ferromagnetic material and are safe for patients to undergo MRI scans at 1.5T and 3T (14,15). Therefore, MRI offers great potential as a single imaging modality and non-radiation based alternative to CT for postoperative assessments.

Unlike for plain radiographs, a factor that affects postoperative image quality of both CT and MRI is the presence of metal related artifacts caused by the fracture fixation implants. These artifacts degrade the image quality and often obstruct the bone and articular structure from being visualised, thus preventing clinicians from assessing the quality of surgical reduction. In CT, metal artifacts are typically seen as bold and starburst streaks resulting from beam hardening, partial volume effects and missing projection data (16). Susceptibility artifacts in MRI are seen as bright and dark blotches in images due to signal mismapping and dephasing (17). The volume of these artifacts also depend on the size, shape, composition and the position of the implants with respect to the X-ray beams and magnetic fields of CT and MRI scanners respectively (18). In spite of these shortcomings, recent studies have reported that suitable CT and MRI protocols can significantly reduce the amount of such artifacts, therefore help to minimise the amount of image distortions (16,17,19-23).

Although CT is often implicated with high radiation dosages, there have been recent technical advancements in the medical manufacturing industry with the development of suitable algorithms and protocols specifically catering for dose reduction (24) while at the same time aiming to preserve image quality (25). An example is the iDose protocol (Philips Medical Systems) utilised in this study. iDose utilises low energy and low dose contrast imaging, and is an iterative reconstruction technique capable of personalising the image quality depending on the needs of patients (26). From the same manufacturer, a post-processing algorithm is also available for the metal artifact reduction for orthopaedic implants (O-MAR) to effectively reduce the amount of metal artifacts generated from orthopaedic implants and subsequently minimize image degradation and distortions (27).

There are numerous studies that have assessed the extent of metal related artifacts for different imaging modalities, implant materials, implant types and anatomical regions (16,18,28,29). Most of these studies have focussed on 2D qualitative assessments. Although Moon *et al*. [2008] have quantified the 3D volume of metal artifacts in CT, a volumetric measurement on its own does not provide information of the dimensions of the artifact. To the best of our knowledge, there are no published manuscripts that specifically quantify and compare optimally reduced metal artifacts of common orthopaedic screws for pilon fracture treatment across three clinical imaging modalities (CT, 1.5T MRI and 3T MRI).

Therefore, the first objective of this study was to develop a simple method for the quantitative assessment of metal screw artifacts in 3D and in relation to the articular surface of the tibial pilon. The second objective was to apply this method to quantify and investigate the effects of imaging modality, screw type and material on the extent of the resulting metal related image artifact.

Materials and methods

Preparation of specimen

One female fresh frozen intact human cadaver specimen

(knee to foot) was acquired from the body bequest program at the Medical Engineering Research Facility (MERF), Queensland University of Technology (QUT). The age of the specimen was 90 years old, and amputated from a left leg. The specimen was kept frozen at –20 ℃ at all times except for scanning sessions and surgical procedures.

This specimen was defrosted 24 hours prior to the surgical insertion of metal screws. An L-shaped incision of about 6 cm in the anterolateral approach was made with a surgical blade to expose the tibial plafond. Utilising the C-arm fluoroscope for imaging and with the aid of K wires, three holes were drilled with a diameter of 2.8 mm at three different distances proximal to and along the distal tibial articular surface.

Three metal screws of the same type and material were inserted into the holes. For this study, four different types of metal screws (Synthes, Oberdorf, Switzerland), commonly used in combination with small fragment locking plates, were investigated: titanium alloy (TA) $TiAl_6Nb_7$ self-tapping locking screw, stainless steel (SS) self-tapping locking screw (thread Ø =3.5 mm, length =40 mm); cannulated TA (CTA) long threaded screw, and cannulated SS (CSS) long threaded screw (thread Ø =4.0 mm, empty core Ø =2.6 mm, length =40 mm).

After the insertion of the screws, the skin flaps were closed with nylon thread, and the specimen was sealed in two plastic bags. The specimen was first scanned on all modalities with TA screws. Subsequently they were replaced with a set of SS screws and the specimen was rescanned. The same process was repeated for the cannulated screw sets.

Acquisition of CT and MRI data

CT

The specimen was positioned on the scan table by aligning the long axis of the tibia with the long axis of the CT scanner (Philips Brilliance 256-slice CT).

The following CT protocols were used: Tube voltage of 120 kVp, X-ray tube current of 190 mA, slice thickness of 1 mm, slice spacing of 0.5 mm, B convolution kernel, thus giving a resulting voxel size of 0.21 mm × 0.21 mm × 0.5 mm. The iDose function (low dose) was used for all of the CT scans. However, O-MAR post-processing was only applied for the TA and CTA screws as pilot scans showed that screws made of steel introduced grey streaks, thus reducing instead of improving the image quality.

The images were saved in the digital imaging and communications in medicine (DICOM) format.

MRI

The specimen was positioned on the bed with the spine array in place and covered with a body matrix receive coil. Following localizer images, sagittal images were aligned along the long axis of the tibia using the 3D FLASH VIBE sequence with the following parameters: TR =11 ms, TE =1.87 ms, number of averages =2, flip angle =10°, pixel bandwidth =488, FOV = 120 mm × 140 mm, slice thickness =0.5 mm, reconstruction matrix =512×256 pixels, in-plane resolution =0.5 mm × 0.5 mm.

This process was repeated with the 1.5T MRI scanner (Siemens Magnetom Avanto) using the same protocols as the 3T MRI (Siemens TRIO).

Reconstruction of 3D bone and metal artifact models

All the CT and MRI data acquired was imported into the image processing software, Amira 5.3 (VSG, France). Based on a semi-automatic threshold method developed by Rathnayaka [2011], the segmentation of bony contours was applied to reconstruct the 3D bone models. This process was repeated again to segment the boundary of the metal artifact so as to generate representative 3D models. After that, all 3D models were saved in STL-format for importing into reverse engineering software (Rapidform 2006, INUS Technology, Korea) for conducting the quantitative 3D assessment of the artifacts.

Alignment of screw models

To quantify metal artifacts produced from each type of screw, the alignment of 3D screw models relative to the metal artifact models must first be established so that the measurements for the extent of metal artifacts can be calculated from the central axis of the screw to the boundary of the artifact in four orthogonal directions with respect to the distal tibia for each dataset.

To correctly position the screws relative to the CT scans, TA screws were used as a reference by aligning the three screw models (provided by Synthes GmbH) in the centre of the artifact model with a trackball function. The position of the screw models was subsequently validated against the CT images (*Figure 1*). This position was replicated for all other CT data by using a fine registration function to align the screw models to the CT-generated bone models. Fine registration is based on the iterative closest point algorithm (ICP) (30,31) (*Figure 1*).

For the positioning of all the screws in MRI scans, the fine registration function was used to align the MRI-

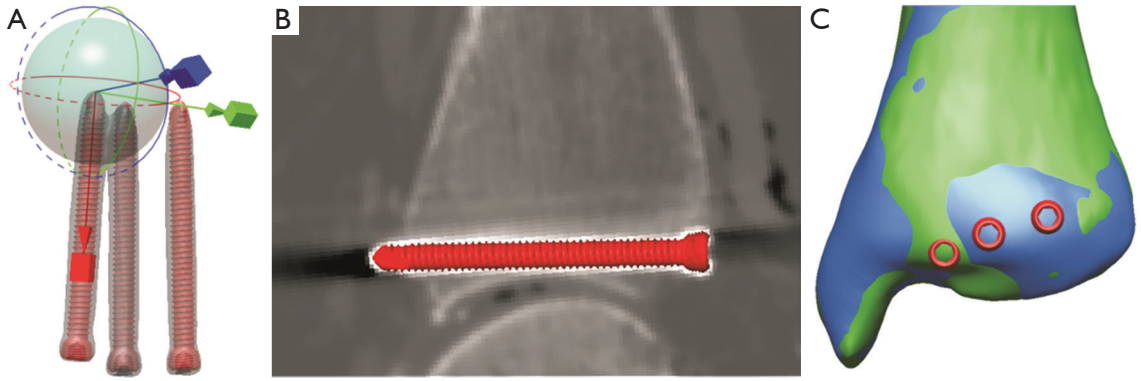

Figure 1 Three screw models were aligned relative to their corresponding metal artifact using a trackball function in Rapidform 2006, after which their correct positions were verified by importing them into Amira 5.3 to be checked against the computed tomography (CT) image. Then, to align them relative to their respective CT bone model (in green), a fine registration function was used in Rapidform 2006. As for the alignment of the MRI bone model (in blue) together with its corresponding screws, they were registered with respect to the CT bone model, and the correct screw positions were again validated against the magnetic resonance imaging (MRI) data in Amira 5.3. (A) Positioning of screws using the trackball function; (B) Verifying the correct position of the screw relative to the CT image; (C) Alignment of CT (in green) and MRI (in blue) bone model using the fine registration function.

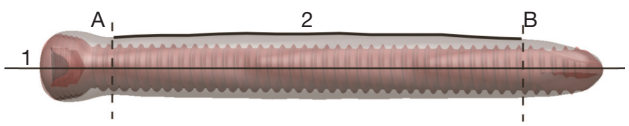

Figure 2 Fitting a curve (numbered 2) along the artifact medially with respect to the central axis of the screw (numbered 1). The same process was repeated to create curves in the lateral, superior and inferior directions. The two rectangular-shaped surfaces (dotted lines named A and B) demarcate the region of interest in the subchondral area of the bone.

generated bone model to the CT-generated bone model, then its screws were positioned relative to the CT bone model. Again, the correct positions of the screws were validated against the MRI data.

The above-mentioned procedure was repeated with three cannulated screw models, and then saved as model files (MDL) for quantitative analysis to be carried out in Rapidform 2006.

Quantitative analysis of metal artifacts

A simple method was developed to conduct a quantitative comparison between the different artifact models in Rapidform 2006. As we are interested in the extent of the artifact in relation to the articular surface of the pilon, we established a coordinate system based on the anatomy of the distal tibia. The artifact measurements were taken approximately perpendicular to the articular surface and in the superior-inferior (SI) direction of the distal tibia following the alignment of the anatomical axis. Measurements in the medial-lateral (ML) direction were taken perpendicular to the anatomical axis. With this coordinate system, the distance between the central axis of the screw to the boundary of the artifact can be measured in four orthogonal directions: superior, inferior, medial and lateral with respect to the distal tibia. Then, two surfaces were demarcated along the body of the screw to serve as a start and end point of the dimensions to be measured, and to focus on the artifacts generated in the subchondral bony region and the distal articular surface. Then, two curves were fitted along the boundary of the artifact in the SI and ML directions and cut using the two surfaces, resulting in four separated curves in the four orthogonal directions.

To measure the perpendicular distance from the central axis of the screw to the boundary of the artifact, the 'Curve/curve Deviation' function was used by selecting the directional curve of interest and the central axis, respectively (*Figure 2*). This function calculates the average distance between all corresponding points along the two curves of interest and its standard deviations.

The same procedure was repeated for the remaining two screws and to all other artifact models. For each artifact model, the average distance was calculated from the four directions, along with its standard deviation. However, as two screws were located in close proximity to each other,

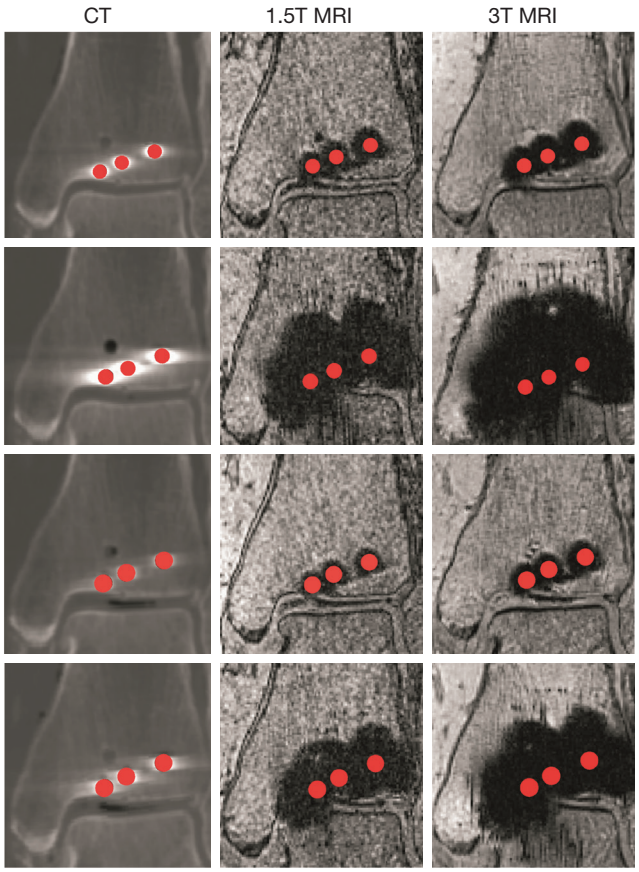

Figure 3 CT and MRI images of the pilon with the inserted screws. First row, TA screws; Second row, SS screws; Third row, CTA screws; Fourth row, CSS screws. Grainy streaks were present in MR images with the steel screws. CT, computed tomography; MRI, magnetic resonance imaging; TA, titanium alloy; SS, stainless steel; CTA, cannulated TA; CSS, cannulated SS.

some artifacts overlapped in between the screws in the ML direction. Therefore, for these cases the measurements in the ML direction were not included.

Statistical analysis

A paired *t*-test with a two-tailed distribution was conducted (Microsoft Excel 2007). This is to assess whether there are significant differences in the size of artifacts generated between the three imaging modalities, screw types and material types. A $P<0.05$ was considered statistically significant.

We have also conducted a repeatability analysis using the 1.5T MRI dataset, for the artifacts generated by the CTA screws. This was done by repeating the segmentation and quantification process, and applying the paired *t*-test between the initial and repeated results.

Results

For all of the imaging modalities and screw types the cross sectional shape of the generated artifacts appeared non uniform relative to the screw centres (*Figure 3*). The mean artifact sizes (in the order of TA, SS, CTA and CSS) from CT were 2.0, 2.6, 1.6 and 2.0 mm; from 1.5T MRI they were 3.7, 10.9, 2.9 and 9 mm; and from 3T MRI they were 4.4, 15.3, 3.8 and 11.6 mm respectively (*Figure 4*).

From *Table 1*, all P values were statistically significant ($P<0.05$) for all imaging modalities except 1.5T versus 3T MRI for the SS screws ($P=0.063$). The artifacts generated by CT were significantly lower than those generated from MRI.

Overall, metal artifacts generated from the 3T MRI were the largest, followed by 1.5T MRI and CT across all four types of screws. Additionally, cannulated screws produced smaller artifacts compared to non-cannulated for all three imaging modalities.

The repeatability analysis showed that the artifact size for the CTA screws from 1.5T MRI was 3.2±0.3 mm. We compared this with the results from our study (2.9±0.3 mm), and found that there were small differences of 0.3 mm, but they were statistically insignificant ($P=0.18$).

Discussion

Achieving anatomical reduction of a fractured pilon is fundamental in ensuring a successful surgical outcome. However, the predominant use of radiographs to assess the quality of articular reduction cannot provide an accurate representation of the malreduced fragments. A potential alternative is the use of CT and MRI as they can provide a 3D representation of the distal articular surface. Nevertheless, orthopaedic implants have been widely known to distort the quality of these medical images, and the impact of these artifacts on the visibility of the articular surface remains uncertain. Therefore, this study aimed to quantitatively compare the extent of artifacts generated from common orthopaedic screws using a human cadaver ankle specimen.

When comparing the extent of the artifacts with the radius of the screws, three (CT: TA, CTA and CSS) were found to be smaller or of the same size. This suggests that the gap between the surface of these screws and the joint can be about 2 mm away from each other to prevent the artifacts from interfering with the imaging of the pilon. However, the extent of artifacts were larger for MRI (1.5T and 3T MRI: TA and CTA), so the gap should be at least

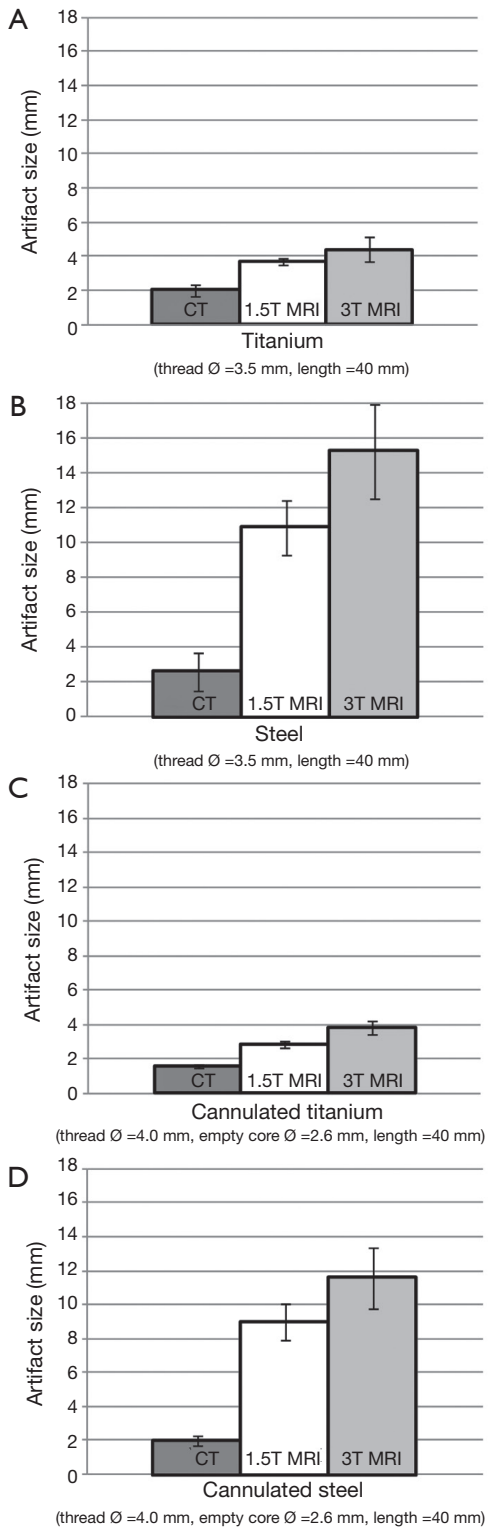

Figure 4 Quantitative comparison on the extent of metal artifacts between the four types of screws and their associated imaging modalities. Distances are measured from the screw axis to the boundary of the image artifact.

3 mm. SS and CSS screws were unfeasible for MRI imaging of the pilon as their artifacts were too large and did not allow the articular surface to be clearly visualised (*Figure 3*).

In clinical applications, 3.5 mm cortex screws are typically used for the preliminary reduction and stabilization of articular segments (32). As such, the results of our study can help provide an indication regarding the minimum distance required between the surface of the screw and the joint for a clear visualisation of the pilon by considering the extent of the artifacts and its associated screw radii.

This study has also shown that the artifacts generated from 3T MRI were larger than from 1.5T MRI, and this was similarly observed in two other studies (18,19). However, it is important to note that the image quality in 3T is higher compared to 1.5T MRI due to its higher signal to noise ratio (SNR) and contrast to noise ratio (CNR) in the distal articular region (20,33), resulting in the production of high resolution MR images of the trabecular bone and tendons in the foot and ankle while at the same time reduce scan times (34). To be able to retain a high resolution image while at the same time generate smaller artifact area in 3T MRI, possible solutions include increasing the readout bandwidth (19,20), incorporating advanced software platforms such as slice-encoding metal artifact correction (SEMAC) and multi-acquisition with variable resonance image combination (MAVRIC) (17), and reducing echo time (18).

One probable source of measurement errors would be due to the non-uniformed shape of the steel-based susceptibility artifacts. They were especially apparent from steel screws scanned using the 3T MRI scanner (*Figure 3*). This would imply that the measurements recorded may vary depending on how the SI and ML reference planes were defined. The shape of the artifacts generated from CT images using TA and CTA screws were also slightly elongated in the ML direction compared to the SI direction in relation to the distal tibia. Nevertheless, even with the small dimensional differences and non-uniformed shape, these would not have provided a negative impact on the obtained outcome because the region we are interested in is the perpendicular distance (SI) between the surface of the screw to the joint for our intended application. According to Schenck (34) and Gill (35), the magnetic susceptibility of SS ($3{,}520\times10^6$ to $6{,}700\times10^6$ ppm) is higher than titanium (182×10^6 ppm), hence directly influences the size of the artifact produced, which may explain why steel-based susceptibility artifacts are larger than those from titanium. Geometric artefact distortions are also evident in these MR

Table 1 Statistical significance of measurements

P values	Titanium	Steel	Cannulated titanium	Cannulated steel
CT *vs*. 1.5T MRI	0.005	0.006	0.001	0.002
CT *vs*. 3T MRI	0.003	0.013	0.005	0.005
1.5T *vs*. 3T MRI	0.020	0.063	0.027	0.032

CT, computed tomography; MRI, magnetic resonance imaging.

images due to signal shifts from the region of interest, which comes from frequency variations in the magnetic field due to higher and lower gradient locations around the hardware (23,36). Since steel has larger magnetic susceptibility values than titanium, larger frequency variations may be produced, which increases the geometric distortions and result in artifact non-uniformities.

Another probable source of errors could come from the segmentation process. Streaks were found on the MRI images generated from the steel screws, which extended to the talar dome. These streaks appear to be of a different texture compared to the steel susceptibility artifacts, i.e., they were projected as grainy surfaces instead of blotches (*Figure 4*). Then again, although these streaks were removed as they were considered as a separate entity to the metal artifacts, they would not have changed the outcome if they were included because SS was found unsuitable for MRI of the pilon. A potential improvement in image quality would be to utilise the 8-channel or dual channel quadrature extremity foot and ankle coil (17), though this is more suitable for TA and CTA screws. We were unable to assess this due to its unavailability at the time of scan.

Repeating the scans was not possible due to limited funding and access to the scanners. Therefore, a repeatability analysis was conducted. From this, the negligible differences in the size of the artifacts from the CTA screws (1.5T MRI) were found to be 0.3 mm between the reported and repeated results. Since its P value was also insignificant (P=0.18), the small reproducibility errors may be ignored for the rest of the datasets as they would not have affected the clinical outcome of the study. This was supported by several other metal artifact studies (37-41).

CT has been well-regarded as the current gold standard for the acquisition of morphological data for the reconstruction of 3D bone models (42). Even though we report that CT produces significantly lower ($P<0.05$) artifacts compared to MRI, ionising radiation exposure cannot be completely eliminated. Calculation of radiation doses were not included in this study to determine the CT dose index (CTDI), therefore the comparison of doses between standard CT protocols and those with iDose cannot be assessed. However, the post-processing technique iDose allows an improved image quality as it reduces noise in the images. We have compared the standard deviations in relation to noise between the conventional filter-back projection (FBP) technique and iDose, and have found that the values in iDose (9.1) were smaller than FBP (14.0). With the reduction in noise, iDose can potentially help reduce radiation exposure in a patient, though its CTDI values need to be calculated to gain a better understanding.

Cannulated screws near the joint surface produce smaller-sized artifacts, which is advantageous in MR imaging applications. MRI can also be presented as a viable postoperative imaging modality and is appropriate for long term clinical studies and clinical management due to its non-ionising capabilities as long as adequate resolution is used to visualise images of the pilon, and if the screws are further than 3 mm from the joint line. In terms of differences in material properties between titanium and SS, titanium is less stiff than steel, thus beneficial as it promotes fracture healing and lower infection rates (43,44). Although there is emerging trend of using TAs for internal fracture fixation due to its improved biocompatibility compared to SS, both materials satisfy the main clinical outcome of fracture fixation, which are to achieve accurate anatomical reduction of the fracture fragments, stabilise and restore the function of the joint (45). By recognising these factors, surgical and imaging techniques can be further improved to optimise patient care in the future.

Limitations in this study include not examining the extent of metal artifacts from other types of orthopaedic implants. Distal tibia fractures often require a combination of plates and screws for accurate anatomical reduction. However, fixation plates are normally located along the medial malleolus or the anterior-lateral region of the distal tibia as compared to screws which are in closer proximity to the articular surface. In a pilot scan with medial and anterolateral titanium plates, the results showed that the artifacts from the plates did not extend to the articular surface for CT and MRI. Based on this, the extent of

artifacts from screws needs to be prioritised, though the artifacts can be compounded if there are many screws located close to each other.

A few pilon fracture studies have reported that the threshold error for the malreduced fragments is restricted to less than 2 mm displacement from the original anatomical position to prevent post-surgical complications such as schlerosis and osteophytes (46-48). Other biomechanical studies have reported that an articular incongruity as small as 1 mm was found to produce detectable alterations in the stress distributions of the joint and resulted in asymmetrical loading and associated degenerative changes (49-51). CT has shown to detect articular step-offs between bony fragments in the acetabulum (52) and the tibial plateau (53), but proved to be short in the assessment of cartilage thickness in post-pilon fractures (41). In addition, CT exposes a patient to radiation. MRI is not only radiation-free, but also the only modality that truly assesses the articular step between the cartilaginous surface on the various displaced joint fragments, though its accuracy in detecting the displaced cortical fragments need to be further examined.

Some shortcomings of MRI in the clinical setting is that their images are more expensive, usually more difficult to access in terms of resource allocation, and takes a longer time for acquisition versus CT. On the other hand, these would not be an issue for the assessment of reduction and potential arthrosis from post pilon fractures in the orthopaedic out-patient scenario, because there is no absolute urgency to obtain the images. In this case, the surgeon can minimise radiation exposure at the request of acquiring MR images. Based on other studies conducted by the same research group, an MRI scan for the whole leg took about 45-65 mins (13,33), during which the leg was scanned in 4-5 stages of 10-12 min scans. This was tolerated by the volunteers who were able to keep their leg still during the individual scanning stages. This suggests that our MRI protocol of 13 mins can also be tolerated since the duration of the scan is similar to that of the previous MRI studies. However, CT can be an alternative for patients suffering from claustrophobia.

We did not examine the heterogeneities in both the CT and MR images. However, we have kept the technical factors such as the alignment of the screw relative to the long axis of the scanners and the protocols the same, hence the heterogeneities associated with the field of view would remain negligible for the purpose of this study.

We did not assess the size of artifacts with the presence of fractures and with more screws, thus may imply that CT and MRI protocols need to be further optimised to provide an accurate delineation of malreduced fragments. This is the objective of a current follow up study. The outcome of this follow-up study will potentially contribute to minimising or eliminating unnecessary radiation exposure to the patient, help determine the threshold level for the remaining articular incongruities leading to postoperative complications, and ultimately help improve clinical management of patients in the long term.

In conclusion, CT generates significantly smaller artifacts compared to MRI but comes at the expense of exposing a patient to ionizing radiation. 1.5T MRI also generates smaller artifacts compared to 3T MRI and hence presents a favourable alternative when using titanium hardware, though it is important to note that it produces lower image quality versus 3T. Postoperative assessment of pilon reduction in both CT and MRI may be improved by using CTA screws when close to the joint surface, but precaution should be exercised to prevent implant failure. Surgeons need to consider these factors to allow accurate assessment of articular reduction and further improvement of operative techniques.

Acknowledgements

The National Imaging Facility (NIF) at the University of Queensland (Brisbane, Australia) has provided subsidised access for this study; Mr. Ian Mellor has assisted with the handling of the cadaver specimen; Mr. Kimble Dunster has operated the C-arm fluoroscope for the insertion of the screws; The last author has received an industrial scholarship from Synthes GmbH.
Disclosure: The authors declare no conflict of interest.

References

1. Chowdhry M, Porter K. The pilon fracture. Trauma 2010;12:89-103.
2. Müller FJ, Nerlich M. Tibial pilon fractures. Acta Chir Orthop Traumatol Cech 2010;77:266-76.
3. Graves ML, Kosko J, Barei DP, et al. Lateral ankle radiographs: do we really understand what we are seeing? J Orthop Trauma 2011;25:106-9.
4. Marsh JL, Buckwalter J, Gelberman R, et al. Articular fractures: does an anatomic reduction really change the result? J Bone Joint Surg Am 2002;84-A:1259-71.
5. Martin J, Marsh J, Nepola J, et al. Radiographic fracture assessments: which ones can we reliably make? J Orthop

Trauma 2000;14:379-85.
6. Moed BR, Carr SE, Gruson KI, et al. Computed tomographic assessment of fractures of the posterior wall of the acetabulum after operative treatment. J Bone Joint Surg Am 2003;85-A:512-22.
7. Pollak AN, McCarthy ML, Bess RS, et al. Outcomes after treatment of high-energy tibial plafond fractures. J Bone Joint Surg Am 2003;85-A:1893-900.
8. Messmer P, Long G, Suhm N, et al. Volumetric model determination of the tibia based on 2D radiographs using a 2D/3D database. Comput Aided Surg 2001;6:183-94.
9. McKinley TO, Rudert MJ, Tochigi Y, et al. Incongruity-dependent changes of contact stress rates in human cadaveric ankles. J Orthop Trauma 2006;20:732-8.
10. van Laarhoven CJ, Meeuwis JD, van der WerkenC. Postoperative treatment of internally fixed ankle fractures: a prospective randomised study. J Bone Joint Surg Br 1996;78:395-9.
11. Matharu GS, Najran PS, Porter KM. Soft-tissue ankle injuries. Trauma 2010;12:105-15.
12. Rathnayaka K, Momot K, Volp A, et al. Quantification of the accuracy of MRI generated 3D models of long bones compared to CT generated 3D models. Med Eng Phys 2012;34:357-63.
13. Schmutz B, Volp A, Momot K, et al. Using MRI for the imaging of long bones: first experiences. J Biomech 2008;41:S188.
14. Shellock FG. Magnetic resonance safety update 2002: Implants and devices. J Magn Reson Imaging 2002;16:485-96.
15. Shellock FG. Biomedical implants and devices: assessment of magnetic field interactions with a 3.0-Tesla MR system. J Magn Reson Imaging 2002;16:721-32.
16. Lee IS, Kim HJ, Choi BK, et al. A pragmatic protocol for reduction in the metal artifact and radiation dose in multislice computed tomography of the spine: cadaveric evaluation after cervical pedicle screw placement. J Comput Assist Tomogr 2007;31:635-41.
17. Sofka CM. Postoperative magnetic resonance imaging of the foot and ankle. J Magn Reson Imaging 2013;37:556-65.
18. Olsrud J, Lätt J, Brockstedt S, et al. Magnetic resonance imaging artifacts caused by aneurysm clips and shunt valves: dependence on field strength (1.5 and 3 T) and imaging parameters. J Magn Reson Imaging 2005;22:433-7.
19. Koch KM, Brau AC, Chen W, et al. Imaging near metal with a MAVRIC-SEMAC hybrid. Magn Reson Med 2011;65:71-82.
20. Farrelly C, Davarpanah A, Brennan SA, et al. Imaging of soft tissues adjacent to orthopedic hardware: comparison of 3-T and 1.5-T MRI. AJR Am J Roentgenol 2010;194:W60-4.
21. Lu W, Pauly KB, Gold GE, et al. SEMAC: slice encoding for metal artifact correction in MRI. Magn Reson Med 2009;62:66-76.
22. Venook RD, Matter NI, Ramachandran M, et al. Prepolarized magnetic resonance imaging around metal orthopedic implants. Magn Reson Med 2006;56:177-86.
23. Lee MJ, Kim S, Lee SA, et al. Overcoming artifacts from metallic orthopedic implants at high-field-strength mr imaging and multi-detector CT. Radiographics 2007;27:791-803.
24. Linton OW, Mettler FA. National conference on dose reduction in CT, with an emphasis on pediatric patients. AJR Am J Roentgenol 2003;181:321-9.
25. Hamberg LM, Rhea JT, Hunter GJ, et al. Multi–detector row ct: radiation dose characteristics. Radiology 2003;226:762-72.
26. Healthcare P. iDose4. 2012. Available online: http://www.healthcare.philips.com/main/products/ct/products/idose/ad/
27. Philips H. Metal artifact reduction for orthopaedic implants (O-MAR). 2012. Available online: http://clinical.netforum.healthcare.philips.com/us_en/Explore/White-Papers/CT/Metal-Artifact-Reduction-for-Orthopedic-Implants-(O-MAR)
28. Moon SG, Hong SH, Choi JY, et al. Metal artifact reduction by the alteration of technical factors in multidetector computed tomography: a 3-dimensional quantitative assessment. J Comput Assist Tomogr 2008;32:630.
29. Holton A, Walsh E, Anayiotos A, et al. Comparative MRI compatibility of 316L stainless steel alloy and nickel-titanium alloy stents: original article technical. J Cardiovasc Magn Reson 2002;4:423-30.
30. Besl PJ, McKay ND. A method for registration of 3-D shapes. IEEE Trans Pattern Anal Mach Intell 1992;14:239-56.
31. Lee YS, Seon JK, Shin VI, et al. Anatomical evaluation of CT-MRI combined femoral model. Biomed Eng Online 2008;7:6.
32. Ruedi TP, Buckley RE, Moran CG. eds. AO Principles of Fracture Management 2. New York: Thieme, 2007.
33. Rathnayaka K, Momot KI, Coulthard A, et al. Anatomical MR imaging of long bones: Comparative performance of MRI at 1.5 T and 3 T. Biomed Spectrosc Imaging 2013;2:21-35.
34. Schenck JF. The role of magnetic susceptibility in

magnetic resonance imaging: MRI magnetic compatibility of the first and second kinds. Med Phys 1996;23:815-50.
35. Gill A, Shellock FG. Assessment of MRI issues at 3-Tesla for metallic surgical implants: findings applied to 61 additional skin closure staples and vessel ligation clips. J Cardiovasc Magn Reson 2012;14:3-7.
36. Hargreaves BA, Worters PW, Pauly KB, et al. Metal-induced artifacts in MRI. AJR Am J Roentgenol 2011;197:547-55.
37. Ernstberger T, Heidrich G, Klinger HM, et al. Score based assessment of implant-related post fusion MRI artifacts focused on different interbody disc spacers: an in vitro study. Open J Clin Diagn 2012;2:23-9.
38. Jedenmalm A, Nilsson F, Noz ME, et al. Validation of a 3D CT method for measurement of linear wear of acetabular cups: a hip simulator study. Acta Orthop 2011;82:35-41.
39. Koff MF, Shah P, Koch KM, et al. Quantifying image distortion of orthopedic materials in magnetic resonance imaging. J Magn Reson Imaging 2013;38:610-8.
40. Olivecrona L, Olivecrona H, Weidenhielm L, et al. Model studies on acetabular component migration in total hip arthroplasty using CT and a semiautomated program for volume merging. Acta Radiol 2003;44:419-29.
41. Thomas TP, Van Hofwegen CJ, Anderson DD, et al. Utility of double-contrast multi-detector CT scans to assess cartilage thickness after tibial plafond fracture. Orthop Res Rev 2009;2009:23-9.
42. Rathnayaka K, Sahama T, Schuetz MA, et al. Effects of CT image segmentation methods on the accuracy of long bone 3D reconstructions. Med Eng Phys 2011;33:226-33.
43. Deepak S, Manjula S. Comparison of Titanium bone plates and screws vs. stainless steel bone plates and screws in the management of mandibular fractures–a long term clinical study. Int J Clin Dent Sci 2011;2:S.
44. Arens S, Schlegel U, Printzen G, et al. Influence of materials for fixation implants on local infection. An experimental study of steel versus titanium DCP in rabbits. J Bone Joint Surg Br 1996;78:647-51.
45. Hayes JS, Richards RG. The use of titanium and stainless steel in fracture fixation. Expert Rev Med Devices 2010;7:843-53.
46. Joveniaux P, Ohl X, Harisboure A, et al. Distal tibia fractures: management and complications of 101 cases. Int Orthop 2010;34:583-8.
47. Rüedi TP, Allgöwer M. Fractures of the lower end of the tibia into the ankle-joint. Injury 1969;1:92-9.
48. Tarkin IS, Clare MP, Marcantonio A, et al. An update on the management of high-energy pilon fractures. Injury 2008;39:142-54.
49. Bai B, Kummer FJ, Sala DA, et al. Effect of articular step-off and meniscectomy on joint alignment and contact pressures for fractures of the lateral tibial plateau. J Orthop Trauma 2001;15:101-6.
50. Bruns J, Volkmer M, Luessenhop S. Pressure distribution at the knee joint. Arch Orthop Trauma Surg 1993;113:12-9.
51. Inaba HI, Arai MA, Watanabe WW. Influence of the varus—valgus instability on the contact of the femoro-tibial joint. Proc Inst Mech Eng H 1990;204:61-4.
52. Matta JM. Fractures of the acetabulum: accuracy of reduction and clinical results in patients managed operatively within three weeks after the injury. J Bone Joint Surg Am 1996;78:1632-45.
53. Barei DP, Nork SE, Mills WJ, et al. Functional outcomes of severe bicondylar tibial plateau fractures treated with dual incisions and medial and lateral plates. J Bone Joint Surg Am 2006;88:1713-21.

Cite this article as: Radzi S, Cowin G, Robinson M, Pratap J, Volp A, Schuetz MA, Schmutz B. Metal artifacts from titanium and steel screws in CT, 1.5T and 3T MR images of the tibial Pilon: a quantitative assessment in 3D. Quant Imaging Med Surg 2014;4(3):163-172. doi: 10.3978/j.issn.2223-4292.2014.03.06

